Journal for Educators, Teachers and Trainers
The PROFESIOLab electronic, peer-reviewed, open-access Magazine

ISSN 1989-9572

DOI: 10.47750/jett.2022.13.05.051

Identifying Potent Histone Deacetylase Inhibitors with Blood-Brain Barrier Permeability Using Image-Guided Synthesis

1SRIDHAR RAO MATTAPALLY,
2NAGANABOINA CHANDRAMOHAN

Journal for Educators, Teachers and Trainers, Vol.13 (5)

https://jett.labosfor.com/

Date of Reception: 12 July 2022

Date of Revision: 13 Aug 2022

Date of Acceptance: 20 September 2022

SRIDHAR RAO MATTAPALLY, NAGANABOINA CHANDRAMOHAN (2022). Identifying Potent Histone Deacetylase Inhibitors with Blood-Brain Barrier Permeability Using Image-Guided Synthesis. Journal for Educators, Teachers and Trainers, Vol.13(5). 560-567.

Journal for Educators, Teachers and Trainers, Vol. 13(5)

ISSN1989 –9572

https://jett.labosfor.com/

Identifying Potent Histone Deacetylase Inhibitors with Blood-Brain Barrier Permeability Using Image-Guided Synthesis

1SRIDHAR RAO MATTAPALLY, 2NAGANABOINA CHANDRAMOHAN
12Assistant Professor
DEPT of H&S
Vaagdevi College of Engineering, Warangal, TS, India

ABSTRACT:

Recent studies have shown that several histone deacetylase (HDAC) inhibitors, which are used to study and treat brain disorders, have poor blood-brain barrier (BBB) penetration. Along with the reported poor HDAC potency and selectivity, insufficient brain penetration may also account for the large dosages needed to achieve therapeutic effectiveness. Using an image-guided methodology that includes radiolabeling and parallel synthesis of multiple compounds based on the benzamide HDAC inhibitor MS-275 as a template, we present here the synthesis and evaluation of a new class of highly potent, bloodbrain barrier permeable HDAC inhibitors for central nervous system (CNS) applications. To maximise BBB penetration, PET imaging and rapid carbon-11 tagging were used in the baboon model. Each chemical's imaging-derived BBB penetration data was then included back into the design process. After examining 17 distinct compounds, it was found that a few of them exhibited high BBB permeabilities and binding affinities. One essential element in this benzamide series that allowed BBB penetration was a basic benzylic amine. The substances showed a 1–100 nM inhibitory impact on recombinant human HDAC1 and HDAC2. Three of the carbon-11 labelled aminomethylbenzamide derivatives showed significant BBB penetration (~0.015%ID/cc) and regional binding heterogeneity (high in the thalamus and cerebellum) in the brain. Together, these techniques have yielded a strategy and a prediction model for developing potent, BBB-permeable HDAC inhibitors for the central nervous system as well as novel, potential compounds for small molecule probes and drugs..

KEYWORDS: Benzamides, blood-brain barrier permeability, positron emission tomography, and histone deacetylase.

INTRODUCTION

Development, inflammation, heart disease, cancer, and neuropsychiatric diseases, such as depression, Alzheimer's disease, and drug use disorders, are all linked to the epigenetic control of gene expression via enzymatic alteration of DNA and histone proteins. DNA methylation and chromatin modifications are two frequent and significant epigenetic changes that produce phenotypic variety without altering DNA sequence by offering a means of passing along environmental cues to the next generation of cells. The histone-modifying enzymes histone acetyl transferase (HAT) and histone deacetylase (HDAC) catalyse the addition and removal of acetyl to control gene expression.

groups from histone proteins' lysine groups, which combine with DNA to create chromatin. By hydrolysing the acetamido group of lysine residues' ε-carbon, HDAC eliminates an acetyl group from histone proteins. This creates a strong charge-charge connection between DNA and histone proteins, making the DNA unusable for transcription factor binding and suppressing gene expression. While deacetylation is connected to gene repression by compressing the chromatin and reducing the amount of DNA accessible for transcription, histone acetylation is generally linked to stimulation of gene expression by exposing DNA to transcription factors.

HDAC comes in eleven isoforms and four classes (I, II, III, and IV). While class II HDACs (4, 5, 7, 9 subtype) and class IV HDACs (HDAC 11 subtype) are present in both the cytoplasm and the nucleus, class I HDACs (1, 2, 3, 8 subtype) are typically located in the nucleus. All HDACs, with the exception of Class III HDAC, have a zinc ion in the substrate binding pocket where the acetamide bond is hydrolysed. HDACi, or class I HDAC inhibitors, have been developed as possible cancer treatments. For the treatment of cutaneous T-cell lymphoma, suberoylanilidehydroxamic acid (1, SAHA, Zolinza, Figure 1A) was authorised as the first medication that targets pan HDAC.7. Furthermore, when combined with traditional cancer medications, SAHA has been clinically investigated for a variety of malignancies, including gliomas and breast cancer. Recent clinical studies have also shown the therapeutic effectiveness of MS-275 (6, Entinostat, Figure 1A), a benzamide form of HDACi, in treating estrogen-positive breast cancer.10. A growing number of studies are assessing HDACi for illnesses of the central nervous system (CNS), including schizophrenia, neurodegenerative disorders, seizures, depression, and addiction, despite the fact that they were first studied for the treatment of cancer.11–15 Reversing aberrant cell transcription instead of addressing downstream translational endophenotypes is one possible benefit of HDAC medications. We looked at the brain absorption of many well-known HDAC inhibitors as possible models for the creation of very powerful blood-brain barrier (BBB) permeable HDAC inhibitors for CNS applications because of the possible therapeutic advantages that HDACi could provide in CNS illnesses. In our early research, we measured the brain absorption and whole-body pharmacokinetics of the well-known HDAC inhibitor medications butyric acid, valproic acid, and 4-phenylbutyric acid using carbon-11 labelled versions of these medications.16 Valproic acid, which has been used for decades to treat seizure disorders, is one of the medications with CNS uses. However, their BBB permeability is quite low. In a similar vein, we discovered that when given intravenously to nonhuman primates, the benzamideHDACi MS-275 (6) had poor brain uptake,17 indicating that it may not be a suitable treatment for CNS diseases. Although in vitro investigations revealed that SAHA might be used therapeutically for CNS applications, Hanson et al.18 recently showed that the absence of behavioural effects of SAHA is likely owing to inadequate BBB permeability. It is obvious that a methodical methodology is required to more accurately forecast the BBB penetration of small molecule probes and medications for CNS therapies, including HDACi.19. Because HDAC isoforms 120 and 221,22 are relevant to CNS disorders, we present a synthesis, radiolabeling, and assessment of extremely effective and BBB permeable HDAC inhibitors guided by PET images. The HDAC inhibitor MS275 served as the model for our series (6, Figure 1A). Despite not being BBB permeable, MS-275's relatively low molecular weight (MW) and nonionic structure at physiological pH allow for the manipulation of several parameters, and the addition of easily labelled functional groups made it possible to use PET to quickly measure brain absorption. Simultaneously, we evaluated the compounds with the greatest brain absorption for their in vitro HDAC inhibitory efficacy.

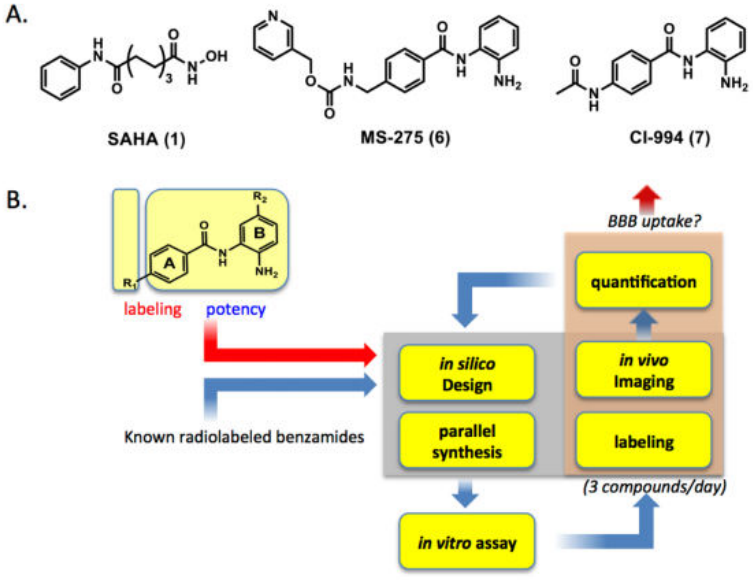

Figure 1. Known HDAC inhibitor drugs (A) and the flowchart for image-guided systematic approach (B).

RESULTS

Overview. The development of a BBB permeable HDAC inhibitor is based on an iterative plan with four components: in silico structural design and prediction, parallel synthesis and in

Table 1. Inhibition Assay of HDAC1, HDAC2, and HDAC3 (IC_{50}, nM)

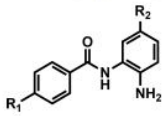

	R_1	R_2	HDAC1[a]	HDAC2	HDAC3
1 (SAHA)	-	-	0.001(0.003)	0.004	0.005
6 (MS-275)	-	H	0.059(0.040)	0.153	0.486
7 (CI-994)	CH_3COCH_2	H	0.045(0.027)	0.031	0.02
8	CH_3COCH_2	2-thienyl	0.002(0.002)	0.002	0.42
9	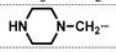	Cl	8.87	6.01	6.5
10	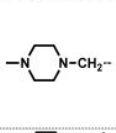	Cl	5.09 (5.5)	1.88	13.3
11		H	0.30	0.62	1.4
12		F	0.22	0.23	-
13		Br	-	-	-
14		I	21.9	10.5	9.8
15	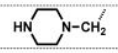	Phenyl	0.006(0.002)	0.023	17.2
16	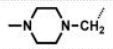	Phenyl	0.005(0.002)	0.022	15.5
17		4-F-C_6H_5	10.2	1.3	2.3
18	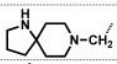	C_6H_5	0.019(0.006)	0.022	17.3
19	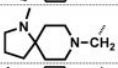	C_6H_5	0.038(0.003)	0.102	9.34
20	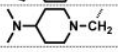	C_6H_5	0.036(0.003)	0.090	22.9
21	NH_2CH_2	H	0.76	2.54	8.21
22	$(CH_3)NHCH_2$	H	0.045(0.005)	0.23	2.55
23	$(CH_3)_2NCH_2$	H	0.47	0.87	0.83
24	NH_2CH_2	C_6H_5	-	-	-
25	$(CH_3)NHCH_2$	C_6H_5	0.025	0.03	13.5
26	$(CH_3)_2NCH_2$	C_6H_5	0.010(0.003)	0.02	5.2
27		4-F-C_6H_5	0.036	0.071	-
28		2-thienyl	0.01(0.003)	0.02	3.76

[a]Recombinant histone deacetylase (the value in parentheses was obtained after 3 h incubation).

vitro HDAC assay, radiolabeling, quantification, and in vivo imaging (Figure 1B). Briefly, as a starting point, four known highly potent HDAC drug candidates and their derivatives (7, 8, 19) including [11C]MS-275 (6) 17 were labeled with C-11 and their BBB permeability was evaluated by in vivo PET imaging. This first set of data was used to generate initial guidelines for structural modification, compared with calculated log BB (BB, ratio of brain to plasma concentration of drug in steady state (Supporting Information (SI) Table 1).23 Then, based on these results, the next set of compounds were designed under the consideration of parallel synthesis, radiolabeling, and in vitro assay. In general, three radiolabeled compounds were designed at a time, creating one set for in vivo evaluation and generating a quantitative structure−property relationship (QSPR) model (SI). The accumulated set of benzamides provided determinant physicochemical properties to be modified for further optimization. We used baboon (Papio Anubis) as it is expected to be similar to human24 and allows more accurate blood analysis at multiple time points than rodent. Chemistry: Structural Design, Synthesis, and Radiochemistry. Despite the low BBB permeability of [11C]MS-275, the core benzamide structure was chosen as a template for our systematic approach varying polar surface area (PSA), charge, molecular volume (MV) (SI Table 1), and lipophilicity.25 Structurally, substituent modification of benzamides was confined at R1 of phenyl ring A and at R2 of phenyl ring B (Figures 1B and 2) because both positions have been shown to be critical for HDAC.26 Among various PET isotopes, carbon11 was chosen in that its 20.4 min half-life made multiple PET studies possible in 1 day in the same animal. For facile and rapid labeling with carbon-11, N-methylation was adopted using [11C]methyl iodide27−29 or [11C]methyl triflate.30 In some cases, N-acetylation was also performed with [11C]acetyl chloride.31 Initially, we chose two known benzamides,32,33 CI-994 (7, Tacedinaline) and 8, both of which have low molecular weight

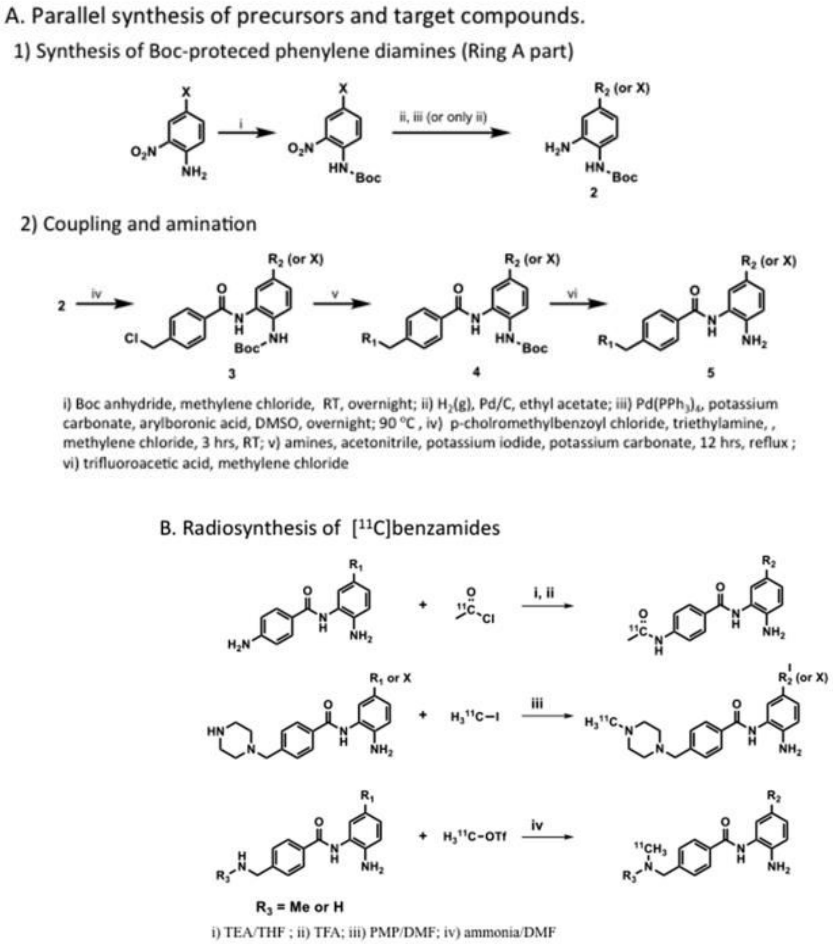

Figure 2. Parallel synthesis and radiolabeling of benzamides.

and sub micromolar HDAC inhibitory activity (Table 1).

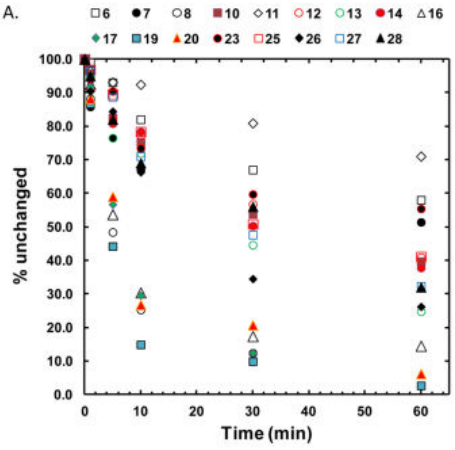

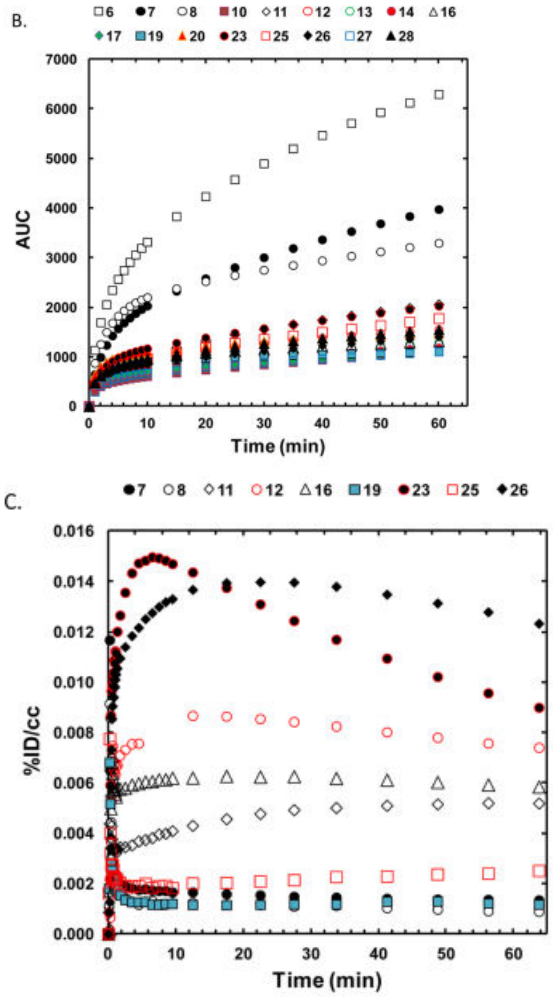

Figure 3. Fraction of unchanged carbon-11 labeledbenzamides (A), area under the curves in baboon plasma over 60 m in after time of injection (B), and time−activity curves of global brain uptake for the selected benzamides (C).

Considering both in vitro binding potency and BBB permeability, we chose compound 26 to evaluate binding specificity to brain HDACs. In the baseline studies, the brain

Table 2. Brain Total Distribution Volume and AUC Ratio of Brain to Plasma for Selected [11C]Benzamides

compd	log $D_{7.4}$[a]	cLogP	PSA[b]	V_T (mL/cm^3)	B_{AUC}/P_{AUC}
6, MS-275	1.8	2.5	119.2	0	0.14
7, CI-994	1.0	1.5	98.0	0.41	0.26
8		3.0	98.2	0.22	0.24
16	2.2	3.8	70.2	8.02	3.54
19	4.7	5.4	70.1	4.81	0.93
20		4.8	70.0	1.35	0.77
23		2.2	64.8	5.51	3.93
25		4.0	74.8	2.13	0.90
26	2.1	4.2	64.8	11.96	7.53
28		3.9	64.8	17.81	5.95

[a]Measured. [b]Polar surface area (Å).

distribution of [11C]26 was heterogeneous, showing highest VT in thalamus, cerebellum, and striatum. A repeated baseline study of [11C]26 on the same day in the same animal showed less than 10% of averaged variability of global brain uptake (n = 3). We examined the regional VT change of [11C]26 caused by pretreatment with unlabeled compound 26 (1 mg/kg) or the potent HDAC inhibitor, SAHA (1 mg/kg) (Table 3). The degree of VT reduction ranged 8−24%, compared with the baseline studies in various brain regions.

Table 3. Difference of Total Distribution Volumes (V_T) of Test−Retest and Blocking Study (n = 3)[a]

	test/retest	pretreatment with SAHA	pretreatment with 26
CB	12.6 (±23.5)	−2.5 (±26.8)	−13.4 (±18.4)
TH	−3.9 (±14.6)	−15.4 (±11.1)	−12.9 (±27.0)
TEMP	3.1 (±19.8)	−8.9 (±20.7)	−24.8 (±5.7)
STR	−4.5 (±21.6)	2.5 (±36.0)	3.8 (±48.5)

[a]CB, cerebellum; TH, thalamus; TEMP, temporal cortex; STR, striatum.

METHODS

[11C]26radiosynthesis. Using an automatic PETtraceMeIMicrolab (GE Medical Systems, Milwaukee, WI) apparatus, [11C]carbon dioxide generated by the 14N(p,α)11C nuclear reaction on an EBCO cyclotron (TR-19, EBCO Industry Ltd., Richmond, Canada) was transformed into [11C]methyl iodide. This was subsequently transformed into [11C]methyl triflate by passing it over an AgOTf furnace at 190 ± 10 °C.At room temperature, 30 [11C]Methyl triflate was moved by argon flow to a V-shaped reaction vessel (5 mL) that held chemical 25 (1 mg) in DMSO (300 μL). The reaction mixture was purified using reverse-phase HPLC (Column, Phenomenex Luna C18(2), 250 mm × 10 mm; flow rate, 6 mL/min; eluent, ammonium formate solution (0.1 M, water/acetonitrile = 25/75)) after being heated for 3 minutes at 50 °C and diluted with 1 mL of HPLC eluent. A rotary evaporator operating at lower pressure was used to collect and concentrate the necessary product (retention duration of 40 minutes). After being reconstituted with 4 mL of sterile saline, the product was filtered into a sterile, pyrogen-free vial using a sterile filter (Acrodisc 13 mm with 0.2 μm HT Tuffryn Membrane, Pall Co., Ann Arbour, MI). After the bombardment ended, the total synthesis time was 75 minutes. Radiochemical purity was >99% (specific activity = 5-18 Ci/μmol at the conclusion of bombardment), and radiochemical yield was 40% (n = 16, decay adjusted). Analytical HPLC (Column, Phenomenex Luna C18, 250 mm × 4.6 mm; flow rate, 1.0 mL/min; eluent, ammonium formate solution (0.1 M, water/acetonitrile = 32.5/67.5; retention duration, 11 min)) was used to assess radiochemical purity and identification. HDAC Inhibition Assay in Vitro. Purified HDACs were incubated for 60 minutes at room temperature in HDAC assay buffer containing 50 mM HEPES (pH = 7.4), 100 mMKCl, 0.01% BSA, and 0.001% Tween-20 with 2 μMcarboxyfluorescein (FAM)-labeled acetylated or trifluoroacetylated peptide substrate (Broad Substrate A and B, respectively) and test compound. The addition of the well-known pan HDAC inhibitor LBH-589 (panobinostat) at a final dose of 1.5 μM stopped the reactions. Following electrophoretic separation of the substrate and product, the Labchip EZ Reader was used to measure and analyse the fluorescence intensity as well as the substrate and product peaks. For every sample, the reactions were carried out twice. Using the 4 Parameter Logistic Model, Origion8 automatically determined the IC50 values. Plotting the percentage inhibition versus the chemical concentration allowed Origin 8.0 software to calculate the IC50 value by fitting the logistic dose-response curve. Starting at 33.33 μM, compounds were evaluated in triplicate using a 12-point dosage curve and a 3-fold serial dilution. PET research on baboons. The Brookhaven Institutional Animal Care and Use Committee gave its approval for the animal experiments. Nine female baboons (Papioanubis, 13.5–21 kg) were used for PET experiments. In short, ketamine hydrochloride (10 mg/kg) was injected intramuscularly to produce anaesthesia, which was subsequently maintained throughout the PET scan using isoflurane (Forane, 1−4%), nitrous oxide (1500 mL/min), and oxygen (800 mL/min). The brain was placed inside the Siemens high-resolution HR+ PET scanner's range of vision. After injecting each labelled substance into a vein in the radial arm, arterial blood was drawn via the popliteal artery and subjected to HPLC analysis. For 90 minutes, each PET scan was conducted in 3D mode, tracking body temperature, respiration rate, and heart rate. For two minutes, arterial blood samples were taken every five seconds. After each radiotracer injection, samples were taken five, ten, twenty, thirty, sixty, and ninety minutes later. Two injections were performed on the same day in the same baboon, either with or without pretreatment of compound 26 (bolus, 1 mg/kg, 20 min prior to radiotracer injection) or SAHA (1 mg/kg, intravenous infusion for 30 min prior to the labelled compound) in order to assess the reproducibility and specificity of compound [11C]26.

CONCLUSION

We thank Michael Schueller for cyclotron operations and Donald Warner for PET operations. We also thank Tiffany St. Bernard, John Dobbs Jr., and Samuel Wilson for their assistance, since the BNL summer internship program helped them with their synthesis work. We used two computational chemistry software programs from the Centre for Molecular Modelling (http://cmm. cit.nih.gov) and Helix Systems (http://helix.nih.gov) at the National Institutes of Health, Bethesda, MD.

REFERENCES

(1) Bernal, A. J., and Jirtle, R. L. (2010) Epigenomic Disruption: The Effects of Early Developmental Exposures. Birth Defects Res., Part A 88, 938−944.

(2) Bierne, H., Hamon, M., and Cossart, P. (2012) Epigenetics and Bacterial Infections. Cold Spring HarborPerspect. Med. 2,x DOI: 10.1101/cshperspect.a010272.
(3) Majumdar, G., Adris, P., Bhargava, N., Chen, H., and Raghow, R. (2012) Pan-Histone Deacetylase Inhibitors Regulate Signaling Pathways Involved in Proliferative and Pro-Inflammatory Mechanisms in H9c2 Cells. BMC Genomics 13, 709−728.
(4) Esteller, M. (2007) Cancer Epigenomics: DNA Methylomes and Histone-Modification Maps. Nat. Rev. Genet. 8, 286−298.
(5) Tsankova, N., Renthal, W., Kumar, A., and Nestler, E. J. (2007) Epigenetic Regulation in Psychiatric Disorders. Nat. Rev. Neurosci. 8, 355−367.
(6) Hyman, S. E. (2012) Target Practice: Hdac Inhibitors for Schizophrenia. Nat. Neurosci. 15, 1180−1181.
(7) Mann, B. S., Johnson, J. R., Cohen, M. H., Justice, R., and Pazdur, R. (2007) FDA Approval Summary: Vorinostat for Treatment of Advanced Primary Cutaneous T-Cell Lymphoma. Oncologist 12, 1247−1252.
(8) Ramaswamy, B., Fiskus, W., Cohen, B., Pellegrino, C., Hershman, D. L., Chuang, E., Luu, T., Somlo, G., Goetz, M., Swaby, R., Shapiro, C. L., Stearns, V., Christos, P., Espinoza-Delgado, I., Bhalla, K., and Sparano, J. A. (2012) Phase I-II Study of Vorinostat Plus Paclitaxel and Bevacizumab in Metastatic Breast Cancer: Evidence for VorinostatInduced Tubulin Acetylation and Hsp90 Inhibition in Vivo. Breast Cancer Res. Treat. 132, 1063−1072.
(9) Lee, E. Q., Puduvalli, V. K., Reid, J. M., Kuhn, J. G., Lamborn, K. R., Cloughesy, T. F., Chang, S. M., Drappatz, J., Yung, W. K. A., Gilbert, M. R., Robins, H. I., Lieberman, F. S., Lassman, A. B., McGovern, R. M., Xu, J. H., Desideri, S., Ye, X. B., Ames, M. M., Espinoza-Delgado, I., Prados, M. D., and Wen, P. Y. (2012) Phase I Study of Vorinostat in Combination with Temozolomide in Patients with High-Grade Gliomas: North American Brain Tumor Consortium Study 04−03. Clin. Cancer Res. 18, 6032−6039.
m. 49, 4616−4622.